

The turbulent/non-turbulent interface bounding a far wake

By DAVID K. BISSET¹†, JULIAN C. R. HUNT²
AND MICHAEL M. ROGERS³

¹Center for Turbulence Research, Stanford University, Stanford, CA 94305, USA

²Departments of Space & Climate Physics and Geological Sciences, University College London,
and J.M. Burgers Centre, Technical University of Delft, The Netherlands

³NASA Ames Research Center, Moffett Field, CA 94035, USA

(Received 17 August 2000 and in revised form 16 August 2001)

The velocity fields of a turbulent wake behind a flat plate obtained from the direct numerical simulations of Moser *et al.* (1998) are used to study the structure of the flow in the intermittent zone where there are, alternately, regions of fully turbulent flow and non-turbulent velocity fluctuations on either side of a thin randomly moving interface. Comparisons are made with a wake that is ‘forced’ by amplifying initial velocity fluctuations. A temperature field T , with constant values of 1.0 and 0 above and below the wake, is transported across the wake as a passive scalar. The value of the Reynolds number based on the centreplane mean velocity defect and half-width b of the wake is $Re \approx 2000$.

The thickness of the continuous interface is about $0.07b$, whereas the amplitude of fluctuations of the instantaneous interface displacement $y_I(t)$ is an order of magnitude larger, being about $0.5b$. This explains why the mean statistics of vorticity in the intermittent zone can be calculated in terms of the probability distribution of y_I and the instantaneous discontinuity in vorticity across the interface. When plotted as functions of $y - y_I$, the conditional mean velocity $\langle U \rangle$ and temperature $\langle T \rangle$ profiles show sharp jumps at the interface adjacent to a thick zone where $\langle U \rangle$ and $\langle T \rangle$ vary much more slowly.

Statistics for the conditional vorticity and velocity variances, available in such detail only from DNS data, show how streamwise and spanwise components of vorticity are generated by vortex stretching in the bulges of the interface. While mean Reynolds stresses (in the fixed reference frame) decrease gradually in the intermittent zone, conditional stresses are roughly constant and then decrease sharply towards zero at the interface. Flow fields around the interface, analysed in terms of the local streamline pattern, confirm and explain previous results that the advancement of the vortical interface into the irrotational flow is driven by large-scale eddy motion.

Terms used in one-point turbulence models are evaluated both conventionally and conditionally in the interface region, and the current practice in statistical models of approximating entrainment by a diffusion process is assessed.

† Present address: SMME, University of Surrey, Guildford GU2 7XH, UK.

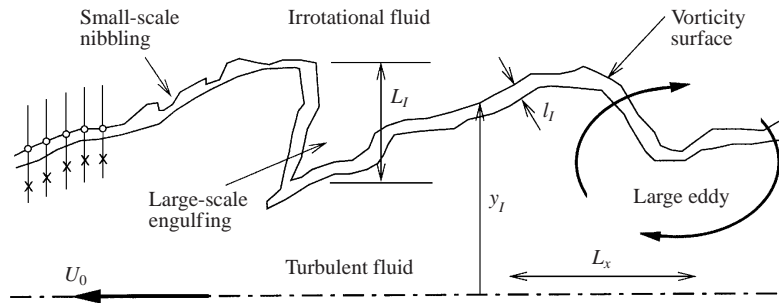


FIGURE 1. The intermittent zone. L_I , l_I , y_I and L_x are sketched roughly to scale. Vertical lines on the left typify data selected for y -direction conditional averaging relative to detection points (\odot) on the vorticity surface; data at a particular displacement $y - y_I$ from the surface, e.g. \times , are averaged to form one point in the conditional average of any quantity, e.g. $\langle U \rangle(y - y_I)$.

1. Introduction

Both naturally and artificially occurring types of turbulence tend to be generated locally wherever the flow is most unstable, and are therefore quite inhomogeneous and intermittent in general, as for example in wakes, boundary layers and thermal convection. In the first two of these types of flow there are intermittent zones between the regions of turbulent motion and the adjacent regions where no turbulence is being generated and where its amplitude is negligible. Similar intermittent regions are found within fully developed turbulent flows, as in the third example, because there are local regions of high-intensity turbulence next to those of much lower intensity (e.g. Monin & Yaglom 1971; Townsend 1976). Most of these intermittent zones have similar characteristic features.

First, the intermittent zone (figure 1) is intersected by a thin, generally continuous, randomly moving interface whose displacements L_I are of the order of the integral scale L_x of the turbulent region velocity fluctuations. The surface of the interface is in general 'fractal' (Sreenivasan & Meneveau 1986) with a range of approximately independent scales, whose width depends on the value of the Reynolds number. Most of the interface surface is continuous because any lumps that break away are soon reabsorbed (e.g. Hussain & Clark 1981). On the turbulent side of the interface the vorticity ω is non-zero, whereas on the other, non-turbulent, side it is negligible. The interface tends to be a strong vortex sheet for a wake, but may not be for some other flows (Townsend 1976). Where there are mean scalar gradients (e.g. temperature) across the zone, there tends to be a sharp jump in the scalar across the interface (e.g. Alexopolous & Keffer 1971).

Secondly, as a result of both the vorticity on the turbulent side and the irregular shape of the interface, random irrotational velocity fluctuations are induced on the non-turbulent side (Phillips 1955) over a distance of order L_x ; thirdly, the absence of vortical fluctuations on the non-turbulent side affects velocity fluctuations on the turbulent side of the interface, typically over a distance of order L_x (Carruthers & Hunt 1986).

Fourthly, as a result of the inhomogeneous distribution of vorticity, the average displacement of the interface moves towards the non-turbulent region at average entrainment speeds \tilde{E}_b , relative to the local mean velocity field, and E_b , in fixed coordinates (e.g. Turner 1986). If, in the turbulent region, the mean velocity parallel to the interface significantly differs from that in the non-turbulent region as in a planar mixing layer, the thickness of the turbulent region increases so that there has

to be a net entrainment velocity E_V normal to the interface. Then the net boundary entrainment velocity in fixed coordinates is $E_b = (\tilde{E}_b - E_V)$.

In many laboratory experiments a velocity probe has been placed at the edge of a turbulent flow, where its output switches back and forth abruptly between a fully turbulent signal and one that is essentially non-turbulent. As described by Corrsin & Kistler (1955), this observation was first understood in terms of a sharp convoluted boundary by Corrsin (1943). Townsend (1948, 1949) quantified this behaviour in terms of an intermittency factor γ , defined as the proportion of time for which the velocity signal is turbulent. As noted above, irrotational velocity fluctuations are usually found in the non-turbulent flow outside the boundary, and the boundary marks not an absence of velocity fluctuations but a change in the character of the fluctuations from vortical to irrotational. Since vorticity is transmitted to fluid only through the action of molecular viscosity, there must exist, in conjunction with any boundary region of local velocity gradient, a shear layer that is essentially *viscous or laminar in nature*, though it may be extremely thin. This layer was termed the ‘laminar superlayer’ by Corrsin & Kistler (1955), and it is important to distinguish between the superlayer and the turbulent/non-turbulent interface studied in the present paper. The latter, though still very thin, is *a layer of turbulent fluid*, and all major changes between the irrotational outer fluid and the relatively uniform, fully turbulent interior fluid occur across this layer. Conceptually the laminar superlayer forms the outer boundary of the turbulent/non-turbulent interface.

Some fundamental questions about these interfaces and free shear intermittent zones (only partly addressed by this paper) may be summarized as follows.

(a) What is the relation between the local mechanism of turbulence production on the scale of the thin interface, and the larger-scale enfolding motions at the scale L_x ? Is the former less significant than the latter so that the value of E_b is determined less by ‘nibbling’ than by ‘engulfing’ as is generally believed (e.g. Ferre *et al.* 1990)?

(b) What are the relative sizes of the thin interface ℓ_I , its random displacement L_I , and the integral scale of the turbulent region L_x ? Why is the interface so thin and so continuous? Do these scales have some general relationship; for example is ℓ_I related to the Taylor or Kolmogorov microscales, i.e. $L_x Re^{-1/2}$ or $L_x Re^{-3/4}$, depending perhaps on the range of Re of the particular flow?

(c) To what extent does the statistical structure of the velocity fluctuations in the intermittent zone have a locally determined and therefore universal form, or to what extent is it determined by the large-scale motion in the turbulent region, for example the profile of the mean vorticity (e.g. Townsend 1976)?

Experimental measurement of an interface in stably stratified flow by Strang (1997) showed that velocity fluctuations $U(y) - \bar{U}(y)$ defined with respect to the mean velocity \bar{U} , and other physical variables, had a much smaller variance if plotted relative to the ensemble mean velocity at the same distance $(y - y_I)$ from the instantaneous (or spatially filtered) interface position y_I ; that is, for any variable V ,

$$\overline{(V(y) - \bar{V}(y))^2} \gg \langle (V(y - y_I) - \langle V(y - y_I) \rangle)^2 \rangle. \quad (1.1)$$

One asks whether these conditional profiles are similar for most kinds of random interface. The idealized theory of Phillips (1955) and Carruthers & Hunt (1986) for the profiles of fluctuations near the interface could be applied relative to either the mean level \bar{y}_I or some filtered instantaneous surface \tilde{y}_I , e.g.

$$V = f((y - \tilde{y}_I)/L_I). \quad (1.2)$$

Gartshore, Durbin & Hunt (1983) showed how such models describe the effects on

the velocity statistics of the fluctuating interface. If there is a scale separation (i.e. $l_I \ll L_I$) and if (1.2) is valid, then it follows that the mean profile of a variable \bar{V} in fixed coordinates can be expressed in terms of its profile relative to the interface, equation (1.2), and the probability distribution $P(\tilde{y}_I)$ of the displacement of the interface, i.e.

$$\bar{V} \approx \int \langle V(y - \tilde{y}_I) \rangle P(\tilde{y}_I) d\tilde{y}_I. \quad (1.3)$$

A better understanding of these mechanisms should help to improve approximate statistical models of turbulence in the intermittent zone. In most models (e.g. eddy viscosity or Reynolds stress transport) the Reynolds stresses or other properties such as eddy viscosity ν_t or dissipation rate ϵ decrease gradually to zero (over a scale L_x) in this zone and do not allow for the large-scale dynamical role and ‘intermittency’ (Townsend 1976) of the interface. In some such models (depending on how $\nu_t(y) \rightarrow 0$) the turbulent region cannot spread into the non-turbulent region. Nevertheless, when the model equations are solved by finite difference methods, it is found that even if $V \rightarrow 0$ as $y/L_x \rightarrow \infty$, E_b is non-zero. This is why, as some authors state quite openly, the value of E_b depends on the numerical methods used, e.g. Large, McWilliams & Doney (1994); see also Hunt *et al.* (2001). Other modelling approaches allow for the intermittency $\gamma(y)$, defined as the proportion of time (or distance) that a point lies on the non-turbulent side of the interface. However, they do not account for the variation of the turbulence relative to the interface. This suggests that a robust physically based statistical model for the intermittent zone has not yet been found! Also see Cazalbou, Spalart & Bradshaw (1994) on this question.

Experimental studies have described many aspects of the intermittent zone, but certain areas are still lacking, especially the three-dimensional structure of the randomly moving interface and the nearby vorticity. Various detector signals have been used to separate turbulent and non-turbulent zones for zone-averaging purposes; for example, Kovaszny, Kibens & Blackwelder (1970) used the level of $(\partial/\partial t)(\partial u/\partial y)$, which responds to fluctuations in spanwise vorticity, to separate vortical and non-vortical zones in the outer part of a boundary layer. If the turbulent zones are heated, the interface can be distinguished with an array of cold wires, as was done by Chen & Blackwelder (1978) in a boundary layer, and by LaRue & Libby (1974), Fabris (1979), and Antonia *et al.* (1987a) in a far wake. A few methods based on streamwise derivatives have been developed, for example $(\partial^2 u/\partial t^2)^2 + (\partial u/\partial t)^2$ applied to a mixing layer by Wygnanski & Fiedler (1970). These references are only a small sample, and there is also an extensive flow visualization literature from which information about interface shapes can be obtained. However, in none of these experimental techniques can the interface position and orientation be tracked while all velocity components are simultaneously measured at high resolution.

Databases from direct numerical simulations (DNS) of turbulent shear flows at reasonable Reynolds numbers now provide an opportunity to bypass some of the experimental difficulties. In this paper the outer boundaries of turbulent zones, defined as the lowest level of vorticity magnitude that can be detected reliably, are delineated in two three-dimensional fields from DNS of far wakes with and without initial forcing (amplification) of two-dimensional low-frequency modes. The flow to either side of the wake is heated to different temperatures so that there is a scalar gradient across the wake. Properties of the flow (including the scalar) in the vicinity of the vorticity surface are determined through conditional averages, leading to the definition of a fairly distinct turbulent interface region. Typical examples of instantaneous flow

patterns and critical points are displayed, especially to illustrate the entrainment mechanism. Terms needed for the equations of a Reynolds-averaged Navier–Stokes (RANS) model of the wake based on the conditional averages are compared to the same terms based on conventional averages, with possible implications for RANS modelling of free-shear flows.

2. Procedure

2.1. The data

Two fields of data from direct numerical simulations of temporal wakes (Moser, Rogers & Ewing 1998) were examined in detail. These simulations, in which the mean velocity $\bar{U}(y, t)$ does not vary in the flow direction, approximate very closely the spatially growing far wake behind a thin flat plate with well-developed turbulent boundary layers, mounted in the plane at $y = 0$. In order to initialize these incompressible spectral simulations, data sets from two instants in a previous boundary layer simulation were placed back-to-back (without the walls) at time zero, and then allowed to develop temporally with streamwise and spanwise periodic boundaries. After some time the initial sharp cusps in the mean velocity and turbulence profiles decayed, and the flow then developed in an approximately self-similar manner until the turbulent region eventually became too large for the computational box in the spanwise direction. One of the simulations was unforced, while in the other case weak forcing was applied, where all two-dimensional modes in the same initial state were magnified at $t = 0$; see Moser *et al.* (1998) for details. Figure 2 gives a visual indication of the differences caused by the forcing.

The first data field examined here is taken from the unforced case at a time t within the final stages of self-similar development. The non-dimensional time $\tau = tU_d^2/\dot{m} = 91.5$, where U_d is the initial centreplane velocity deficit and \dot{m} is the integrated mass flux deficit divided by density and spanwise (z) length. The second field comes from the weakly forced simulation at $\tau = 90.3$, well within the self-similar region for that case. Moser *et al.* (1998) show that growth rates and turbulence levels for the two cases are just below (unforced) and just above (forced) typical ranges found in far-wake experiments that do not involve explicit forcing. In both cases the Reynolds number $Re_{\dot{m}} = \dot{m}/\nu$ is 2000, which is high enough for sustained fully turbulent flow. Results are normalized by U_0 , the centreplane mean velocity deficit, and b , the half-mean-velocity width across both sides of the wake; the Reynolds number U_0b/ν is approximately 2000 also. The stored spectral data were projected onto uniform physical grids of $387 \times 400 \times 97$ (unforced) or $387 \times 500 \times 97$ (forced) points for further processing, giving the physical grid data about the same resolution as the spectral. In all figures the free-stream flow is zero on average, and therefore the velocity deficit flow is right-to-left, i.e. negative. The equivalent flow in a wind tunnel would include a large free-stream velocity from left to right, which is therefore the downstream direction.

A passive scalar quantity T with a Schmidt or Prandtl number of 0.7 was included with the simulated flow. Its values were 1.0 in the upper free stream and 0 in the lower, creating a scalar gradient across the entire flow, and it was initialized to a smooth profile across the turbulent region ($T = f(y)$ only). Thus, initially, there was only an approximate correspondence between non-vortical fluid and free-stream values of the scalar, but it became closer over time because of mixing within the wake and entrainment of the surrounding fluid. The fact that the two free-stream values are different is very useful for determining the origin (above or below the wake

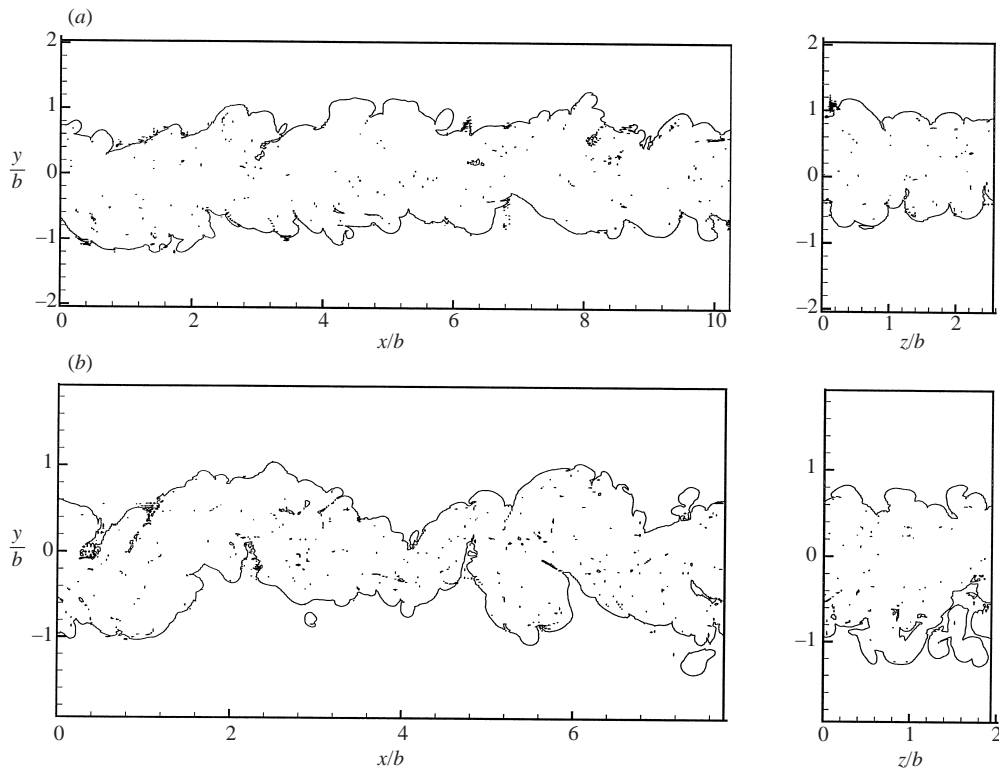


FIGURE 2. Contours of vorticity modulus ω in (x, y) - and (z, y) -planes at the levels used for detection of vorticity surfaces. (a) Unforced wake, $\omega = 0.7U_0/b$; (b) weakly forced wake, $\omega = 1.2U_0/b$.

centreplane) of any enclosed or re-entrant region of non-vortical fluid found near the centreplane. In laboratory experiments, passive scalars such as temperature are used as markers of vortical fluid; an investigation of the use of scalar levels for detection of the interface is reported by Bisset *et al.* (1998).

2.2. Detection of the turbulent/non-turbulent interface

In a fully turbulent flow such as the present, all vortical fluid is expected to be turbulent, and therefore $\omega = \sqrt{\omega_x^2 + \omega_y^2 + \omega_z^2}$ (the magnitude of the vorticity vector) can be used for detecting the boundaries of turbulent regions. As with all level-based methods, it is important to set the detection threshold appropriately. In laboratory experiments, the inevitable combination of some free-stream turbulence and instrument noise means that measured vorticity is often non-zero in the non-turbulent regions. Where a DNS is computed with a spectral method, background numerical noise has similar consequences, since noise in wavenumber space is equivalent to noise across the entire physical space. Therefore, if the spatial gradient in ω is low at the edges of turbulent fluid, genuine vorticity cannot be distinguished from noise. Raising the detection level would not be the solution; not only would large external areas of vortical fluid be omitted by the detection process, but also the areas of relatively low ω within the vortical fluid would be incorrectly detected as irrotational. On the other hand, it is much easier to detect vortical regions if spatial gradients in ω are quite steep, because a detection level slightly above the background noise can be used, and

the detected interface positions will be almost independent of small increases in that level. Fortunately, the dynamics of vortical interfaces (described later) cause the latter situation to be prevalent, as determined both by plotting contours and by forming conditional averages from different detection levels.

Contours of ω were plotted in several (x, y) - and (z, y) -planes, and it was found that the contour $\omega = 0.7U_0/b$ best delineated vortical regions in the unforced wake. Contours below this level spread out into the free stream in a disorganized fashion; contours above this level tend to fall at very similar positions along the wake edge but also outline many small low- ω regions throughout the wake interior. Examples of contours at this level in (x, y) - and (z, y) -planes are shown in figure 2. Peak ω levels are of order 100 times higher, and the centreplane mean is ten times higher. After inspection of many such contours, $C_\omega = 0.7U_0/b$ was chosen as the detection threshold level in the unforced wake. The same detection level in calculation units was used for the forced wake, although its normalized level ($C_\omega = 1.2U_0/b$) is greater (see figure 2 for contours at this level). In this case too much numerical noise in the free stream was detected at the lower normalized level. Note that the normalized centreplane mean vorticity is also greater for the forced case (e.g. figure 5).

The indicated surface marks the approximate outer boundary of the turbulent/non-turbulent interface, but there is no obvious level of ω that would define an inner boundary of the interface, and in fact it may be impossible to define an interface thickness except in a conditionally averaged sense. However, the main point to be made here is that the detected vorticity *surface* is distinct from the turbulent/non-turbulent interface, a layer of non-zero thickness.

The vorticity surface is quite convoluted and sometimes re-entrant, especially in the forced case (figure 2). The direction in which the surface faces varies continuously. In a few places there appear to be patches of vortical fluid that are completely isolated, although they are actually two-dimensional cuts through three-dimensional protrusions that are attached to the main body out of the planes shown in the figure.

Conditional averaging through the interface requires not only detections of locations of the interface but also knowledge of the direction in which it is facing at each detected position, because conditional averages would be smeared out very quickly away from the detection point if the averaging path made a random angle to the interface. The simplest procedure is to average along a line normal to the interface, and to assume that this line is given by the normal to the detected vorticity surface. Therefore the results presented here are based only on detections of the position and orientation of the outer surface of the interface, which gives a reasonably accurate estimate of the interface position as long as it is not too thick. There are then (at least) two options for the averaging procedure itself: either to average along a different direction (relative to the fixed coordinate frame) for each instance by three-dimensional interpolation, or to collect the detections into groups according to the direction of the normal and average along a fixed direction for each group. Given that the properties of the interface might vary systematically with direction (parallel or normal to the mean shear direction, for example), the latter option was chosen, with the added benefit that it simplifies interpolation.

In order to achieve high resolution of any rapid changes through the interface, detection points are defined at the exact locations where ω reaches the detection threshold C_ω , assuming linear variation of ω between gridpoints. For example, the j th point of N detection points to be used for conditioning in the x -direction is at (x_j, y_j, z_j) , where y_j and z_j are exact multiples of grid spacings Δy and Δz , but $x_j = n_j\Delta x + (\delta x)_j$ (with n_j an integer and $0 \leq (\delta x)_j < \Delta x$). Then the conditional

average $\langle q \rangle(x - x_j)$ of any quantity q is defined as

$$\langle q \rangle(x - x_j) = \frac{1}{N} \sum_{j=1}^N q(x_j + m\Delta x, y_j, z_j) \quad (2.1)$$

where m takes on a suitable range of negative and positive integer values (in other words $(x - x_j)$, the displacement relative to the interface, is only defined in practice for discrete values $(x - x_j) = m\Delta x$). Linear interpolation based on $(\delta x)_j$ is used to find q between gridpoints. Analogous definitions are used for conditioning in the y - and z -directions, and $(y - y_j) = m\Delta y$ is equivalent to the continuous coordinate $(y - y_I)$. The equivalent of conventional time averaging, i.e. averages over all points at specified values of $|y|$, is denoted by an overbar. Another form of averaging, often applied to experimental measurements of intermittently turbulent regions but not used in this paper, is zone averaging (at specified $|y|$ values, averaging all those data points that fall within turbulent zones). Conditional averages of fluctuations are defined relative to the conditional mean values, e.g. the variance $\langle u^2 \rangle = \langle (U - \langle U \rangle)^2 \rangle$, except that in certain cases a comparison is made with the conditionally averaged fluctuation relative to the conventional mean, e.g. $\langle u^2 \rangle = \langle (U - \bar{U})^2 \rangle$ – such cases are pointed out where they occur.

2.3. Selection of interface groups

There is no reason to assume that properties should be similar everywhere on the interface. Therefore a number of interface detection criteria were applied along with the basic vorticity threshold in order to select interface subsets that are similar in given ways. To begin with, the direction in which the vorticity surface is facing was considered. Surfaces roughly normal to the x (streamwise), y (transverse) or z (spanwise) axes were selected, and conditional averages were derived by sampling along lines parallel to the respective axes. In general, data from both sides of the wake were combined, with sign reversal where appropriate, into a single ensemble, but surfaces normal to x were only selected if facing downstream. For selection purposes, the surface angle at any point was determined as follows. For detections of surfaces required to be facing in (say) the y -direction, i.e. making an angle of 90° to the y -axis, the adjacent ω -level detection points in the $\pm x$ -direction were obtained and joined by a line; the process was then repeated for adjacent detections in the $\pm z$ -direction. Both lines were required to make an angle of at least 65° to the y -direction in order for the detection to be accepted. An equivalent description is to say that both the streamwise and spanwise angular errors of the accepted surfaces are within $\pm 25^\circ$. When finding detection points for averaging along the x - (or z -) directions, not only was the surface angle criterion applied, but a detection was accepted only if ω was below the threshold C_ω for an x distance (or z distance) of at least $0.1b$ and then above it for at least the same distance, which avoided detections of numerical noise while allowing for up to sixteen or so detections along a given line.

Additional detection criteria were used for conditional averages in the y -direction, to investigate (i) the effects of distance of the interface from the centreplane, and (ii) areas where the interface is re-entrant, i.e. places where a line in the y -direction passes through more than one distinct vortical zone. In the latter case detections were accepted only if the successive vortical and non-vortical zones along the detection line had lengths of at least $0.07b$, again trying to avoid small patches of noise. Finally, interfaces leaning upstream by 15° to 45° , and then interfaces leaning downstream by the same range of angles, were studied through y -direction conditional averages (the

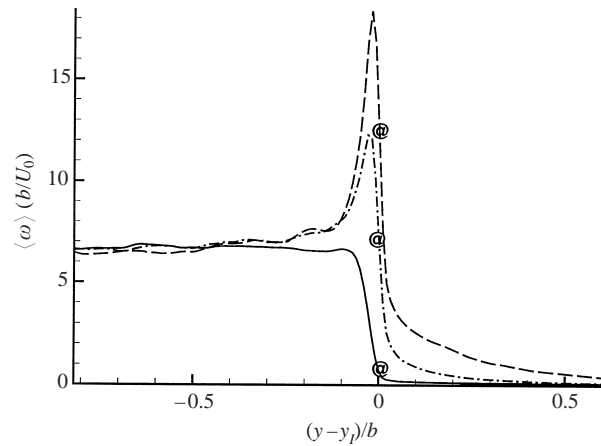


FIGURE 3. Effect of detection threshold C_ω on $\langle \omega \rangle$, unforced wake. Values of $C_\omega b/U_0$ were 0.7, 7.0 and 12.3 at the detection points, indicated by '@'.

angular error spanwise still being limited to $\pm 25^\circ$). Interface groups mentioned in this paragraph are sketched in figure 13, although the relationship between the interfaces in the figure is derived later.

3. Results

3.1. Surface detection level

Vorticity magnitude $\langle \omega \rangle$ conditionally averaged in the y -direction for three values of the threshold C_ω (and surface normal angular errors $\leq 25^\circ$) is shown in figure 3 (unforced wake). When $C_\omega b/U_0 = 0.7$ (the value chosen for our analysis), the proportion of surface area included from each side of the wake, when projected onto the centreplane, is about 26% relative to the centreplane area. In all cases $\langle \omega \rangle$ is almost constant at the same value in the middle part of the wake, and there is a very sharp gradient down through the detection level. There is no restriction on the steepness of this gradient made by the detection process – it only has to be negative. The gradient becomes even steeper with increasing C_ω , but, as figure 3 shows, detection points then start to concentrate on locally intense patches of vorticity, reducing the proportion of data accepted and producing sharp peaks in $\langle \omega \rangle$. More significantly, excessive amounts of vortical fluid leak into the irrotational region when C_ω is large. At lower levels of C_ω than shown, numerical noise is detected too often, and irrotational fluid is included with the vortical region.

3.2. Statistics of vorticity surface height

As noted above, the vorticity surface is not identical to the turbulent/non-turbulent interface – it is only the outer boundary of the interface – but statistics of surface height above the wake centreplane are a good indicator of interface positions. The surface angle criterion is not used here, so coverage of the projected area is 100% in both the forced and unforced wakes. Re-entrant regions are included, counting both the downcrossing and second upcrossing of the ω threshold, and simultaneous intrusions of irrotational fluid from both sides of the wake are allowed for. Since irrotational fluid can cross the wake centreplane (especially in the forced wake), the value of the scalar in re-entrant regions is checked to determine which side of the wake the fluid came from.

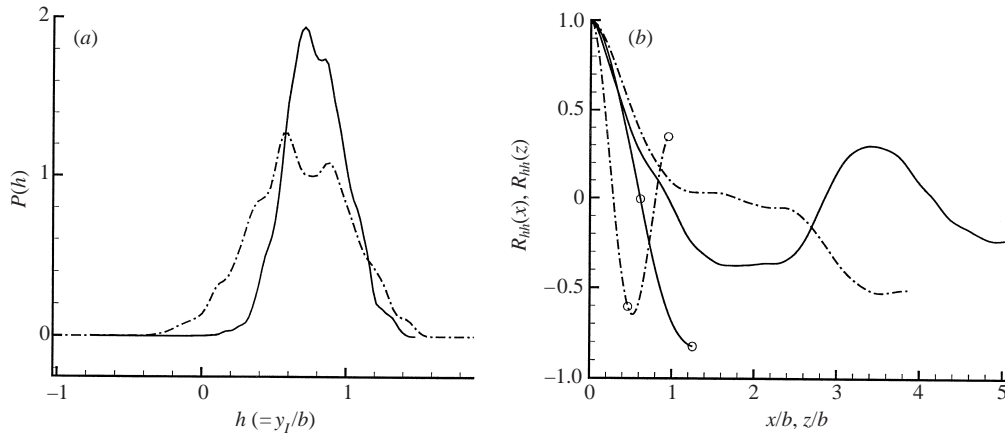


FIGURE 4. Statistics of vorticity surface heights in the unforced (—) and forced (— · —) wakes. (a) Probability density functions; (b) streamwise (plain) and spanwise (marked with circles) autocorrelations.

Figure 4(a) shows probability density functions of vorticity surface heights $h = y_1/b$ for unforced and forced cases. The mean height for the unforced (forced) case is 0.79 (0.68), the standard deviation 0.21 (0.33), skewness 0.03 (−0.12), and flatness factor 3.28 (2.78). Thus to a first approximation h is a normal random variable, where the main effect of forcing, as could be expected from figure 2, is to spread out the range of heights towards the centreplane and sometimes across it. It is not clear whether the small dip in the $P(h)$ curves is repeatable or only related to the particular starting field for these simulations. Re-entrant zones on one side of the wake (either upper or lower) occurred over 7% (16%) of the centreplane area, and occurred on both sides simultaneously for 0.1% (2%) of centreplane area, for the unforced (forced) case.

Autocorrelation coefficients $R_{hh}(x)$ and $R_{hh}(z)$ for the two cases are presented in figure 4(b); here the inner detections in re-entrant regions are omitted. The usual practice for correlations is followed in regard to treatment of the mean, i.e. the mean height is subtracted, so the resulting autocorrelation curves emphasize the length scales of the variations in surface height that produce the p.d.f. curves in figure 4(a). Note that because of the periodic boundary conditions the ranges of correlation displacements can only extend over half the lengths and spans of the actual realizations in figure 2. The dominant streamwise scale for height fluctuations in the unforced wake is about $3.4b$, which is determined from the peak in the correlation curve shown in figure 4(b). This value agrees very well with the scale of organized motion outside a far wake implied by figure 4 of Antonia, Shah & Browne (1987b), bearing in mind their definition of length scale $L = b/2$. That figure also shows that the dominant scale is considerably larger outside the wake than within the turbulent zones, which appears to be the case here too. For the present results in figure 4(b), the spanwise scale of interface height in the unforced case and the streamwise scale in the forced case have become too large to be determined within the available correlation distance. In the forced wake, however, the spanwise scale has become so large, as a result of the two-dimensional forcing, that the scale of local height fluctuations (about $1.1b$) shows up quite clearly.

It can be inferred from figure 3 that the average level of ω is constant throughout turbulent zones of the wake, and equal to the centreplane mean value of vorticity magnitude ω_0 . Therefore the Eulerian distribution of $\bar{\omega}$, with its long tails, is determined

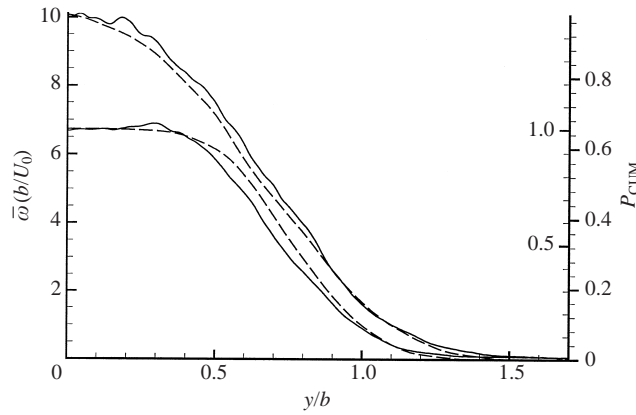


FIGURE 5. Cumulative probability of interface height (---) compared to mean vorticity magnitude (—) in the forced (upper curves) and unforced (lower curves) wakes. The two P_{CUM} axes are scaled so that the respective curves match at the centreplane.

solely by the wake’s convoluted bounding surface. Following equation (1.3),

$$\bar{\omega}(y/b) = \omega_0 \int_{y/b}^{\infty} p(h)dh. \tag{3.1}$$

The validity of this assumption can be checked by comparing $\bar{\omega}$ with the intermittency distribution (rescaled by a suitable constant), as shown in figure 5. In this figure the p.d.f. curves of figure 4(a) have been integrated from $h = y/b$ to $h = h(\text{max})$ to derive the ‘intermittency factor’, i.e. the cumulative probability P_{CUM} that h is greater than y/b , and rescaled to match $\bar{\omega}$ at the centreplane. The curves agree quite well for both forced and unforced cases, the discrepancies being less than ℓ_1 ($\approx 0.07b$), the thickness of the interface determined in §3.4. Similar agreement can be expected for other properties that scale with vorticity, such as dissipation rate. This result supports the concept of turbulence in the intermittent zone being determined by two features (Townsend 1976): (a) fully turbulent fluid whose vorticity is well mixed within the turbulent zone, and (b) a convoluted envelope created by large-scale eddy motion. However, it should be recalled that vorticity, as a function of velocity derivatives, is dominated by smaller scales; other turbulence properties (e.g. velocity fluctuations) that include contributions from large-scale motion may be distributed less uniformly within the turbulent zones.

3.3. Effect of surface orientation

As mentioned above, about 26% of centreplane area is below areas of the vorticity surface that are facing nearly vertically for the unforced wake (about 21% for the forced wake). This means that substantial areas face in other directions, and therefore it is important to know whether surface orientation has any significant effects on interface properties. Distributions of $\langle \omega \rangle$ for both wakes are shown in figure 6(a) for surfaces facing in the three principal directions. (The vertically facing interfaces are tilted about 3° upstream on average, and streamwise- and spanwise-facing interfaces average a few degrees above horizontal.) Normalized by U_0/b , a measure of vorticity from the mean shear, $\langle \omega \rangle$ has steeper gradients and reaches higher levels in the forced wake. Differences caused by orientation are much smaller, especially when comparing vertically and spanwise-facing surfaces (the gradient for downstream-facing surfaces is a little weaker in both wakes). The gradual rise in $\langle \omega \rangle$ to the right of the detection

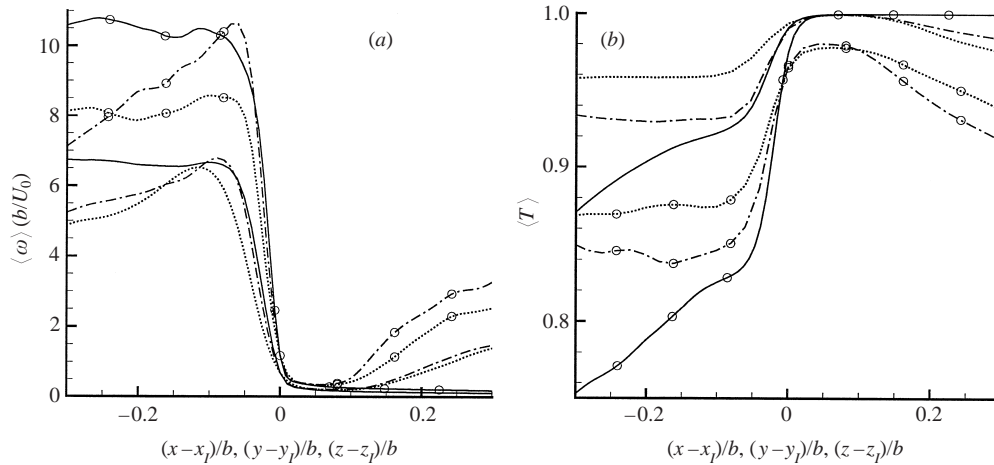


FIGURE 6. Effect of surface orientation on conditional averages of (a) vorticity magnitude and (b) passive scalar in the forced (with circles) and unforced (plain) wakes. Orientation: ·····, downstream; ———, vertically; — · —, spanwise.

point for spanwise- and downstream-facing surfaces is the result of intermittency: lines parallel to the centreplane may intersect many different vortical and non-vortical regions, sometimes quite closely spaced. The decline in $\langle \omega \rangle$ to the left of the detection point (after the initial step rise) has the same cause. Forcing seems to have some effect on the distribution of $\langle \omega \rangle$ for downstream-facing surfaces, reducing (relatively) the level just inside the surface. The common characteristic of all six curves is a sharp, almost linear rise of $\langle \omega \rangle$ for $0.06b$ inside the vorticity surface, followed by a nearly constant- $\langle \omega \rangle$ region from about $-0.08b$ inwards.

Corresponding distributions of temperature $\langle T \rangle$ (a passive scalar) are shown in figure 6(b). The sharp gradient in $\langle \omega \rangle$ at the interface and the constant value in the fully turbulent regime are consistent with generation of vorticity at the interface. But the jump in $\langle T \rangle$, $\Delta \langle T \rangle$, the bulk movement of the interface at a speed E_b , and the absence of any local generation/destruction of temperature (heat), require that there is an eddy flux of heat towards the interface $F_{\theta(t)}$ equal to $E_b \Delta \langle T \rangle$. Since $F_{\theta(t)} \propto -\partial \langle T \rangle / \partial y$, this flux implies that there is a finite gradient of $\langle T \rangle$ on the turbulent side of the interface, as is observed.

Levels of $\langle T \rangle$ for the inner regions are much lower for the forced wake, and consequently the gradients up to the surface are steeper. The strengthened large-scale organized motion rapidly transports fluid from one side of the wake to the other (recall that boundary conditions for T are 1.0 and 0 above and below the wake), and promotes mixing in the interior. This effect is consistent with the fourfold increase in transverse velocity variance reported by Moser *et al.* (1998). It is not as easy to explain the effect of forcing on the streamwise- and spanwise-facing curves just outside the detection point, where $\langle T \rangle$ almost reaches 1.0 in the unforced case but peaks around 0.98 with forcing. When T -contours are superimposed on ω -contours such as those in figure 2, one can see that T occasionally has non-free-stream values while ω drops below C_ω , but such events are larger and occur more frequently in the forced wake. The cause may be related to the imperfect initial matching of T to the vortical fluid, as mentioned earlier.

Concluding this section, it should be noted that the vorticity surface is moving

continuously, so that any differences at a particular point caused by surface orientation will in general be diminished by changes in orientation with time.

3.4. Defining the turbulent/non-turbulent interface

Figure 6 shows that the modulus of vorticity and the mean gradient of temperature are approximately constant in the wake interior (also see figure 3), which means that small-scale turbulence and the eddy diffusivity are fairly uniform across the wake up to the interface. It also shows that the vortical fluid in the wake interior is separated from irrotational fluid in all principal directions by a layer of constant average thickness with strong gradients in vorticity and passive scalar. Across this layer, which differentiates the turbulent and the non-turbulent flow regions, there is a transition from free-stream irrotational fluid to well-mixed vortical fluid, and therefore the turbulent/non-turbulent interface may be defined as this layer. For the present flows, the thickness of the interface (so defined as the region of rapid change) is about $0.06b$ to $0.08b$, which is several times smaller than the standard deviation of the height of its convolutions (§3.2). The interface thickness is comparable to the Taylor microscale λ , but it is an order of magnitude larger than the Kolmogorov microscale. Whether the interface thickness scales with either of these quantities cannot be established until DNS data are available at considerably higher Reynolds numbers. In some of the following figures the position of the interface is indicated by vertical lines using the largest estimate ($0.08b$) of its thickness.

3.5. Some statistical properties of the interface

While figure 6 shows the change in the modulus of vorticity through the interface, it is necessary to consider how velocity gradients and the different components of $\langle \omega \rangle$ are distributed in order to understand the interface dynamics. This also differentiates between the small-scale dynamics which dominate the vorticity components and the large-scale dynamics which influence the conditional velocity components. Conditional magnitudes $\langle |\omega_x| \rangle$, $\langle |\omega_y| \rangle$ and $\langle |\omega_z| \rangle$ are presented for vertically and spanwise-facing interfaces (unforced wake) in figure 7, along with any non-zero gradients of conditional velocity components such as $\partial \langle U \rangle / \partial y$. Magnitudes are more relevant than signed vorticity components because many of the small-scale quantities may have either sign instantaneously, and therefore average to zero. Note that the mean spanwise vorticity is included in $\langle |\omega_z| \rangle$.

The dominant component in vertically facing interfaces (figure 7a) is spanwise vorticity $\langle |\omega_z| \rangle$, and the weakest, being normal to the detected surface, is $\langle |\omega_y| \rangle$. Within the interface itself, especially towards its outer surface, $\partial \langle U \rangle / \partial y$ is nearly as large as $\langle |\omega_z| \rangle$, showing that the variation of velocity at the largest scale is a major contributor to vorticity within the interface. In the main body of the wake, $\langle |\omega_z| \rangle$ is much greater than the mean shear. Note that the small-scale turbulence is approximately isotropic, since the magnitudes of all vorticity components become similar. The distribution of $\langle U \rangle$ from which $\partial \langle U \rangle / \partial y$ was calculated is shown in figure 8.

The general picture is similar for spanwise-facing surfaces (figure 7b), but here $\langle |\omega_z| \rangle$ is the normal component and therefore weakest. Transverse vorticity $\langle |\omega_y| \rangle$ is strongest, and there is a substantial large-scale contribution $\partial \langle U \rangle / \partial z$. Streamwise vorticity $\langle |\omega_x| \rangle$ is also strong, with a modest large-scale contribution $\partial \langle V \rangle / \partial z$. For streamwise-facing surfaces (not shown) the strongest component is $\langle |\omega_z| \rangle$, and $\partial \langle V \rangle / \partial x$ makes a moderate contribution. Forcing the wake has no major effect on the overall pattern of vorticity distribution, though relative magnitudes vary a little (results not shown).

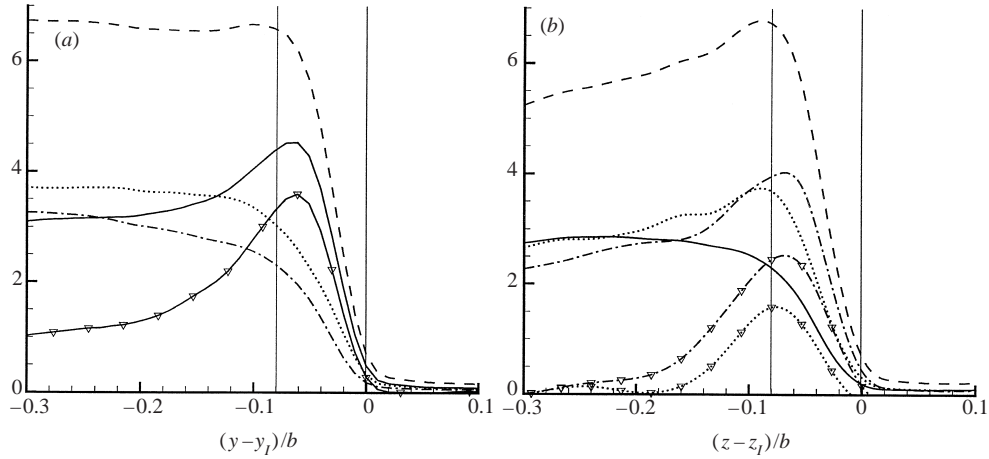


FIGURE 7. Vorticity components and significant velocity gradients for interfaces facing (a) vertically, and (b) spanwise, in the unforced wake. All curves are normalized by U_0/b , and velocity gradients are indicated with symbols. — — —, $\langle \omega \rangle$; ·····, $\langle \omega_x \rangle$ and $-\partial \langle V \rangle / \partial z$; — · —, $\langle \omega_y \rangle$ and $\partial \langle U \rangle / \partial y$; — — —, $\langle \omega_z \rangle$ and $\partial \langle U \rangle / \partial y$. Thin vertical lines show interface position.

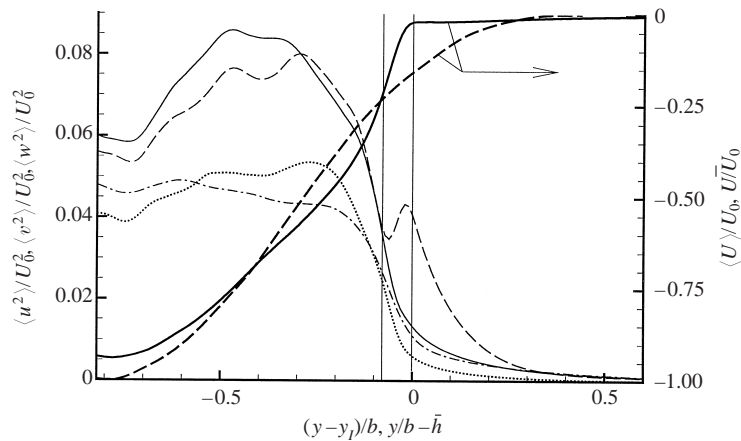


FIGURE 8. Conditional velocity variances relative to conditional means for vertically facing interfaces: — — —, streamwise; — · —, transverse; ·····, spanwise. Also shown: conditional (bold solid) and conventional (bold dashed) mean streamwise velocity, and conditional streamwise variance relative to the conventional mean (— — —). Vertical lines show interface position. The abscissa for \bar{U}/U_0 is $y/b - \bar{h}$.

The unconditional and conditional mean velocity profiles $\bar{U}(y)$ and $\langle U \rangle(y - y_I)$ are shown in figure 8, along with variances of velocity fluctuations, $\langle u^2 \rangle$, $\langle v^2 \rangle$ and $\langle w^2 \rangle$, for vertically facing interfaces in the unforced wake. The approximate interface position is indicated by a pair of parallel lines, and \bar{U} is plotted against $y/b - \bar{h}$ to allow direct comparison with $\langle U \rangle(y - y_I)$. Fluctuations are defined here relative to the *conditional* means, e.g. $u = U - \langle U \rangle$, and for comparison the profile of streamwise fluctuations relative to the conventional mean, i.e. $\langle (U - \bar{U}(y))^2 \rangle$, is also shown. Unlike \bar{U} which varies smoothly near the edge of the wake, $\langle U \rangle$ increases rapidly through the interface until it levels out quite sharply at its free stream value. The effect of this difference between \bar{U} and $\langle U \rangle$ can clearly be seen in the two streamwise variance curves: $\langle (U - \bar{U}(y))^2 \rangle$ increases towards the outer surface, and large values

continue for a distance outside the interface. In other words, \bar{U} is not a good estimate of U at the outer edge of the interface. These high levels of $(U - \bar{U}(y))^2$ make a significant contribution to the conventional (unconditioned) values of $\overline{u^2}$ towards the outer edge of the wake. They are produced by large-scale effects on velocity, i.e. the convolutions of the interface, not by fluctuations associated with small- or medium-scale turbulence.

Spanwise velocity W is also parallel to vertically facing interfaces, but the conventional mean and conditional average are both zero, so there are no systematic large-scale effects. Consequently, values of $\langle w^2 \rangle$ decrease quite quickly through the interface, and there is virtually no difference when \bar{W} is subtracted instead of $\langle W \rangle$. Mean transverse velocity \bar{V} is essentially zero, and $\langle V \rangle$ (not shown) is quite small when all vertically facing interfaces are included as in this figure (subsets are presented later), so $\langle v^2 \rangle$ is also little affected by the choice of mean to subtract.

Variations well outside the interface are still non-zero because of irrotational fluctuations induced by large-scale turbulent motions. Antonia *et al.* (1987*b*), for example, detected large structures inside a far wake at $y = 0.45b$ and found (by conditional averaging) a strong correspondence with irrotational fluctuations outside the wake. Variations inside the wake continue to increase for some distance past the inner edge of the interface (unlike $\langle \omega \rangle$), which is probably because larger-scale turbulence structures, which contribute strongly to velocity variances but not much to ω , cannot be centred close to the surface. Because this flow has mean shear, the streamwise variance is greater than the spanwise at all distances above and below the interface, even when the conditional mean is subtracted from fluctuations – otherwise these two variances would be identical.

It is interesting to compare these results with the idealized theory of Carruthers & Hunt (1986) for the transition zone between homogeneous isotropic turbulence and irrotational fluctuations. They assumed that there is a thin vortical interface which is essentially level, and that there is no mean velocity jump across the interface (i.e. $\Delta\langle U \rangle = 0$) and no mean shear. They showed that the velocity fluctuations are affected by the interface over a distance of order L_x on the turbulent side (predicting that $\langle v^2 \rangle$ decreases while $\langle u^2 \rangle$ and $\langle w^2 \rangle$ increase), while the vorticity varies over the thickness of the interface, which is much less than L_x . Outside the interface $\langle v^2 \rangle$ decreases more slowly, as $(y - y_I)$ increases, than $\langle u^2 \rangle$ and $\langle w^2 \rangle$ (as Phillips 1955 also found). The latter is supported here by the conditional statistics, and also by the results of Antonia *et al.* (1987*b*) for a cylinder wake. If the theoretically predicted profiles are displaced randomly according to the probability distribution $p(h)$ of the interface, as in Gartshore *et al.* (1983), then $\overline{u^2}$, $\overline{v^2}$ and $\overline{w^2}$ can be computed; the maximum $\overline{u^2}$ falls near $y = 0.7b$.

Figure 9 shows $\langle U \rangle$ and $\langle V \rangle$ for spanwise-facing interfaces (over a smaller range of distances because intermittency becomes important for averaging parallel to the centreplane). As for the previous case (figure 8), there is a rapid rise in $\langle U \rangle$ through the interface, which occurs in spite of the lack of mean shear in this direction ($\bar{U}(z)$ is constant). However, $\langle V \rangle$ is also significant in the present case, not only for its contribution $\partial\langle V \rangle/\partial z$ to vorticity within the interface, but also for its negative values at the outer surface and beyond, which indicate that free-stream fluid moves down past the detected surface towards the wake centre. These spanwise-facing interfaces are mainly found on the sides of turbulent protrusions welling up into the free stream, and fluid within the protrusions carries the velocity defect outwards from the centreplane; hence the contrast in $\langle U \rangle$ across the interface.

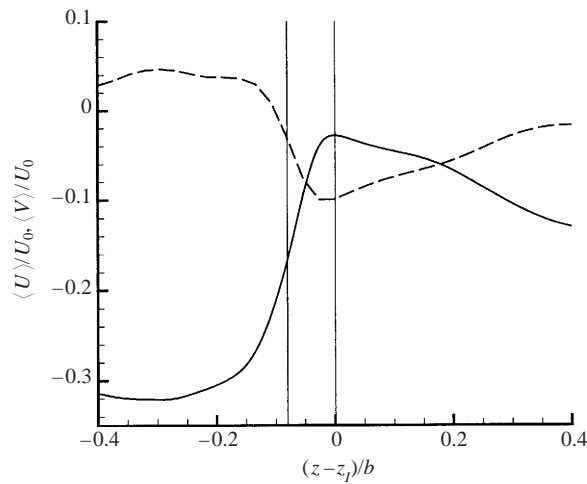


FIGURE 9. Conditional velocities for spanwise-facing interfaces, enforced. —, $\langle U \rangle$; ---, $\langle V \rangle$. Vertical lines show interface position.

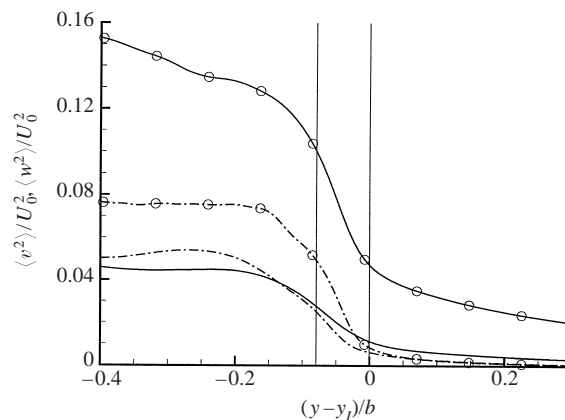


FIGURE 10. Conditional velocity variances for vertically facing interfaces, forced (with circles) and unforced. —, $\langle v^2 \rangle$; - · -, $\langle w^2 \rangle$.

The main effect of forcing the wake is to amplify the fluctuations and therefore the contortions of the interface (figure 2). For vertically facing interfaces, figure 10 displays $\langle v^2 \rangle$ and $\langle w^2 \rangle$ with and without forcing, and it can be seen that the increases differ substantially for different components. For $\langle w^2 \rangle$ the increase is rather less than a factor of two, and even smaller for the irrotational fluctuations above the interface, but $\langle v^2 \rangle$ is quadrupled everywhere. The effect on $\langle u^2 \rangle$ (not shown) is proportionally only a little greater than that on $\langle w^2 \rangle$. These changes are consistent with the effects of forcing on conventional variances found by Moser *et al.* (1998). Because the forcing is primarily two-dimensional, there is a comparatively small effect, not shown here, on the spanwise $\langle V \rangle$ distribution conditioned on spanwise-facing interfaces (figure 9), in contrast to the large increase in $\langle v^2 \rangle$.

3.6. Effects of interface height and slope

From figure 6 it appears that similarities between interfaces with different orientations are more noteworthy than differences, but orientation is only one of the criteria

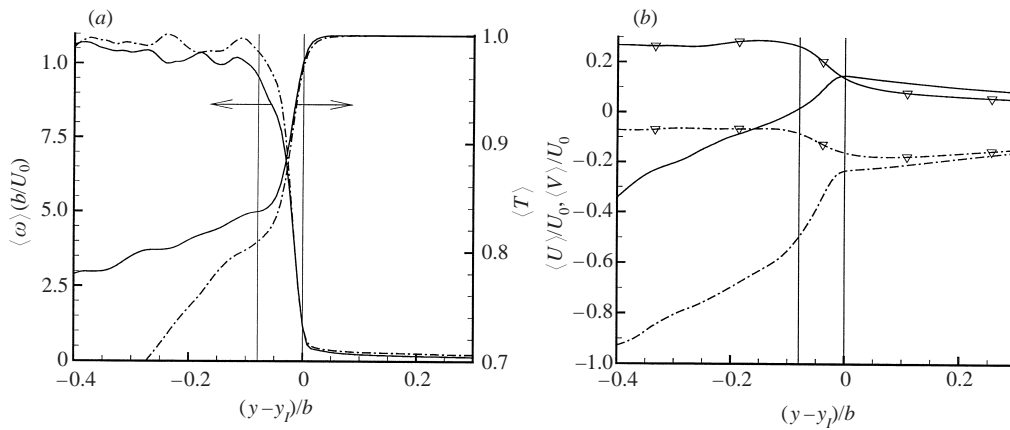


FIGURE 11. Effect of separating interfaces into three groups by height above centreplane, forced wake: —, outer group; - · -, inner group. (a) Conditional vorticity and scalar. (b) Conditional velocities $\langle U \rangle$ (plain) and $\langle V \rangle$ (with symbols). Vertical lines show interface position.

that might affect interface properties. Distance from the wake centreplane could be significant because, for example, the engulfment process is by definition impossible at the outermost edges of the wake, and must occur closer to the centreplane. Interface slope could be important because surfaces leaning upstream (facing partly towards the oncoming free stream) are in different surroundings from those facing partly downstream. These two aspects were examined in the following manner. Results are presented only for the forced wake; the same effects were found (but not as strongly) in the unforced wake.

The set of detections of vertically facing interfaces (as used above) was split into three groups of roughly equal size according to distance from the wake centreplane (h -value). The cutoff values for h were 0.72 and 0.92 (0.62 and 0.93) for the unforced (forced) wake, which may be loosely compared to the p.d.f.s of figure 4(a) bearing in mind that all surfaces are included in the p.d.f.s irrespective of angle. Some results for the inner and outer groups are shown in figure 11. Clearly there is no significant difference in $\langle \omega \rangle$ resulting from the split (figure 11a). Magnitudes of the three components of vorticity (not shown) are also virtually unaffected. The slope of the curve for $\langle T \rangle (y - y_i)$ is required to be steeper somewhere along its range when the interface is much closer to the centreplane, but the profiles show the same jump $\Delta \langle T \rangle$ for both cases and a significant region of constant gradient (different for the two cases) in the body of the wake. Velocity variances (not shown) are only mildly affected by the inner/outer split.

Conditional velocities, however, are affected quite substantially by interface height. Distributions of $\langle U \rangle$ and $\langle V \rangle$ for inner and outer groups in the forced wake are presented in figure 11(b); the effects in the unforced wake are identical in nature but only half the magnitude. Fluid surrounding the outer group, i.e. the extended bulges of the interface, is moving rapidly outwards: $\langle V \rangle$ reaches almost $0.3U_0$ just inside the interface. Irrotational fluid is forced to accelerate to $0.15U_0$ above the mean free stream as it flows around the protrusions (figure 11b), and all fluid within the interface thickness is moving faster than average in the streamwise direction. Just the opposite occurs when the interface is close to the centreplane: irrotational fluid is rushing inwards from the free stream at a speed $0.18U_0$, but it has a horizontal speed of about $-0.23U_0$ relative to the free stream. All of these accelerations and decelerations

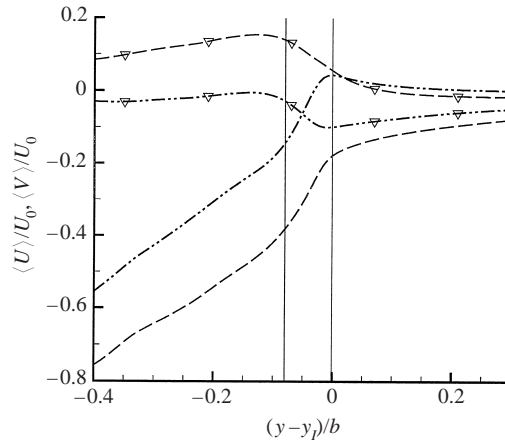


FIGURE 12. Conditional velocities $\langle U \rangle$ (plain) and $\langle V \rangle$ (with symbols) for upstream-leaning (—) and downstream-leaning (---) surfaces. Interface position is shown by vertical lines.

are primarily irrotational, not vortical, and they are all effects of large-scale structural interactions with the free stream.

When interface angle is the selection criterion instead of height, the effect on $\langle U \rangle$ and $\langle V \rangle$ is interestingly different. The selected upstream-leaning group contains all surface detection points for which the normal makes an angular error $\leq 25^\circ$ from vertical spanwise but is tilted upstream in the range 15° to 45° . The downstream-leaning group uses the same range of tilting downstream. Average angles of tilt within both groups were found to be 28° – 30° in the relevant direction (both forced and unforced wakes). However, the total projected area covered by the upstream-leaning surfaces is 50% (forced) or 100% (unforced) larger than the downstream-leaning area. Results for the forced wake are shown in figure 12; results are similar, but less contrasted, for the unforced case. Only velocities are shown since $\langle T \rangle$ was little affected and $\langle \omega \rangle$ was unchanged for these groups. The upstream-leaning group has a fairly strong outwards $\langle V \rangle$, but unlike the outer group (figure 11*b*) its associated $\langle U \rangle$ is well below the free-stream value both within and above the interface. In other words, slow-moving vortical fluid is moving outwards here and has not yet been accelerated by interaction with the free-stream fluid. Conversely, the fluid around the downstream-leaning interfaces is moving inwards, as for the previous inner group in figure 11*b*, but at this point its streamwise velocity is above average instead of much below it.

As with the inner and outer groups, the effects of surface angle are related mainly to large-scale motion. All four types of interface and their associated velocities could be related as shown in figure 13, where they form a general pattern of large-scale rotating regions. They repeat continuously, with variations of spacing, strength and scale, along both sides of the wake. Notice also that there is a tendency for irrotational fluid to force its way underneath the protrusions of vortical fluid, forming zones where the vorticity surface is re-entrant. This aspect is examined next.

3.7. Re-entrant zones

In most places any vertical line passing right through the wake intersects the vorticity surface twice only, but there are places (especially in the forced wake) where a line passes through more than one distinct vortical zone, intersecting the surface four or even six times (see § 3.2 for statistics). Conceivably a patch of irrotational fluid could

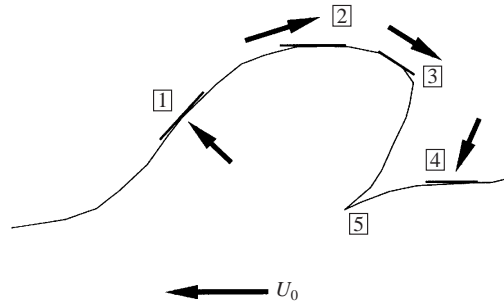


FIGURE 13. Notional arrangement of detected surfaces. Arrows show corresponding typical interface velocities ($\langle U \rangle, \langle V \rangle$) relative to free stream. 1, upstream-leaning; 2, outer group; 3, downstream-leaning; 4, inner group. A re-entrant zone is also indicated (5).

be entirely trapped within the wake, but usually the multiple intersections occur within a re-entrant zone as sketched in figure 13 and readily identified in figure 2. Detection of such zones is straightforward (§2.3), and results in sets of three detection positions: the top of the vortical protrusion, the downwards-facing surface where the interface separates protrusion from irrotational intrusion, and the bottom of the intrusion. Conditional averaging is complicated by the variable heights between detections (the protrusions and intrusions have variable thicknesses) that could cause smearing, and therefore conditional averages were calculated separately for the top, middle and bottom detections. Because of the small total area of interfaces in re-entrant zones, no surface angle criteria were used, which means that the surface normal is often angled well away from the averaging direction (vertical).

Composite conditional averages $\langle \omega \rangle$ and $\langle V \rangle$ for re-entrant zones are presented in figure 14. The '@' indicates detection points on the $\langle \omega \rangle$ curves (figure 14a, unforced wake), showing how the curves (including $\langle V \rangle$) from the top and bottom detections have been offset by $+0.2b$ and $-0.12b$ respectively. These offsets were selected for best visual alignment of the curves where they overlap; the offsets were slightly smaller ($+0.16b$ and $-0.1b$) in the forced wake. The $\langle \omega \rangle$ level in the protrusion itself ($(y - y_I)/b \approx 0.1$) is still remarkably strong, given that in some cases the line of conditional averaging is only glancing the tip of the vortical protrusion. Gradients of $\langle \omega \rangle$ through all three interfaces are nearly as steep as in other cases shown already. Results for $\langle \omega \rangle$ with forcing (not shown) are qualitatively the same.

Curves for $\langle V \rangle$, both forced and unforced cases, are given in figure 14(b). The inwards velocity is very strong for the intruding irrotational fluid, as might be expected, and forcing doubles the speed of intrusion. The streamwise velocity $\langle U \rangle$ (not shown) for all fluid is well below the free-stream value. The most interesting aspect, however, is the great width of the negative- $\langle V \rangle$ region in figure 14(b): it shows that all of the vortical fluid in the protrusion and the bottom interface is also moving rapidly inwards along with the irrotational fluid. Clearly the re-entrant zone is the result of motion on a larger scale than that of the intrusion itself.

What seems to be happening is that when the rotational structure depicted in figure 13 is strong enough and acting for long enough, its inrush on the downstream side pushes irrotational fluid deep inside the body of the wake, stretching out the surrounding interface and carrying along the associated vortical fluid. In general a corresponding strong surge outwards occurs at the upstream side of the rotational structure, bulging and stretching the interface in that area too. Strong gradients within the re-entrant interface are maintained at least in part by the parallel stretching of

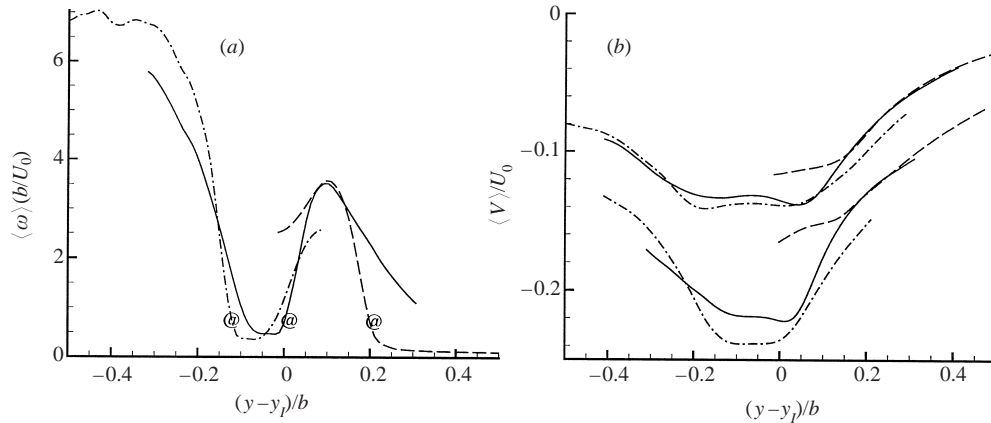


FIGURE 14. Conditional results for re-entrant zones. Surfaces: — — —, outermost; — — —, downwards-facing; - · -, innermost. (a) $\langle \omega \rangle$, unforced wake. Detection points indicated by '@'. (b) Corresponding distributions of $\langle V \rangle$, unforced (upper curves) and forced (lower curves).

the interface, given the absence of mean shear effects in this region. The re-entrant interface nearly always ends in a sharp cusp, the inevitable consequence of local entrainment (i.e. interface advancement into the irrotational fluid normal to its own surface). Some aspects of interface stretching and renewal, and entrainment, are considered in the next two subsections.

3.8. Interface dynamics and the boundary entrainment rate

Results so far have shown that local properties of the interface, at least in a conditionally averaged sense, do not vary greatly for different orientations and positions of the interface. Also it is clear that the interface maintains its properties over time, while entraining fluid into the growing wake (the wake is self-similar with a constant growth rate – see Moser *et al.* 1998 for details). Therefore there must be some persistent mechanisms that maintain the interface in spite of diffusion and internal mixing processes that would tend to dilute its internal gradients and reduce its surface area. By inspection of individual instants of interfaces in the flow, aspects of interface structure can be investigated using the methods of critical point analysis.

Sectional streamlines in flows around interface regions are shown in figure 15 for part of an (x, y) -plane in the forced wake and a (z, y) -plane in the unforced wake. These particular realizations were chosen for their relative clarity, but they are not exceptional. Sectional streamlines are lines that are everywhere parallel to velocity vectors projected onto the given plane – see the review by Perry & Chong (1987). Normally the plane of visualization is itself moving at a reference velocity typical of the fluid, so that streamlines will emphasize local flow structure. The present reference velocities have been chosen so that a velocity zero (critical point) coincides with the ω -surface in a certain area. In fact the exact position of the zero is a free choice, but the resulting pattern of streamlines around the critical point is fully determined by the flow. The number of saddle and nodal points in a plane must be equal, given certain conditions on the edge of the plane (Hunt *et al.* 1978).

In figure 15(a), (x, y) -plane, a critical point of particular interest is the saddle point (stagnation point) S where fast-moving irrotational fluid descends to meet an upflow of vortical fluid. Other critical points (right at the edges of the figure) are nodal foci F within the turbulent fluid upstream and downstream from the saddle, forming a

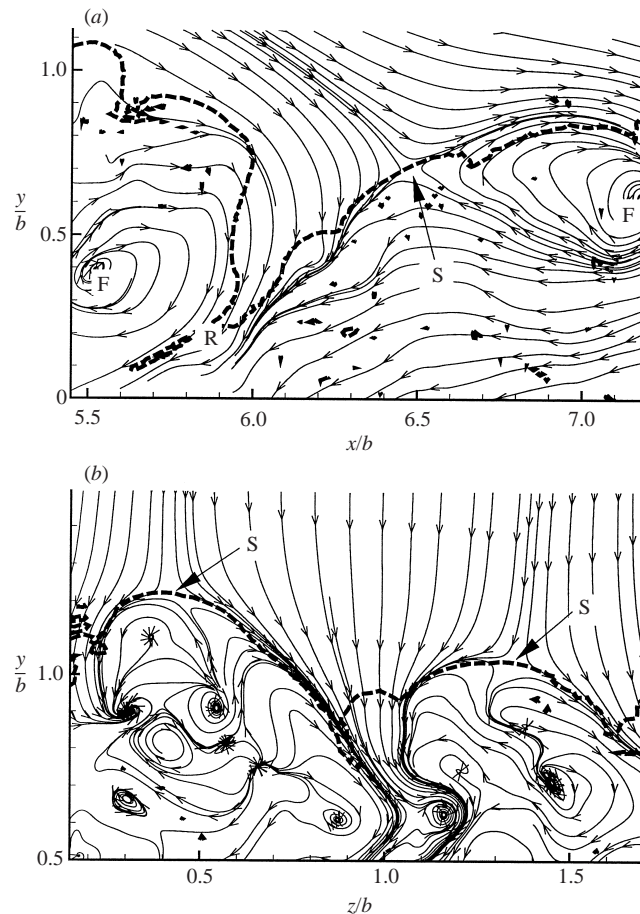


FIGURE 15. Sectional streamlines relative to vorticity surfaces (heavy dashed lines). (a) Part of an (x, y) -plane, forced wake. (b) Part of a (z, y) -plane, unforced wake.

pattern well known from far-wake instantaneous (e.g. Bisset, Antonia & Browne 1990) and conditionally averaged (e.g. Steiner & Perry 1987; Antonia *et al.* 1987a; Bisset *et al.* 1990) velocity fields. In the present DNS, however, the ω -surface is resolved too (the heavy dashed line). Well-mixed, vortical fluid is brought into close proximity with irrotational fluid and stretched out along the interface, which tends to keep the interface thin. The shape of the interface is not static, and vorticity distributed within the turbulent region induces movement of the interface. In general streamlines only cross the interface where the normal to the interface is parallel to its general direction of movement, as with a propagating vortex ring (Turner 1973) or a saddle point in a free shear layer (e.g. Hussain 1986). Where the fluid accelerates away from the stagnation point in both directions roughly parallel to the interface, vorticity is advected by the flow into the re-entrant zone R where mixing and diffusion of vorticity (the final stage of entrainment) occur, and the boundary of vortical fluid moves outwards. This is analogous to the rear stagnation point of a propagating turbulent vortex ring.

A spanwise cut through the wake is shown in figure 15(b), with the frame of reference velocity (directly upwards) chosen to give a zero at the upper edge of the

ω -surface. Fortunately, in this view there are two protrusions rising with the same velocity, so stagnation points (saddles) appear on the tops of both. The protrusions are clearly the results of motion on a fairly large scale. Several critical points appear within the turbulent areas of the protrusions, associated with stable and unstable foci (nodes) and saddles on a smaller scale. As in the (x, y) -plane, streams of rising vortical fluid and descending irrotational fluid meet at stagnation points and then accelerate away roughly parallel to the interface. In the centre of the figure there appears to be a small bridge of older interface material that is being pushed into a deepening fissure.

In summary, cuts through the wake in both directions show how streams of vortical and irrotational fluid collide at the interface, stretch out along it, and drive its convoluted, fissured shape. Large-scale movements (engulfing motions) of the interface are dominant, driven by inviscid dynamics. If, at the Reynolds numbers of the simulations, significant ‘nibbling’ (engulfing motions on very small scales) had been present, the profiles of $\langle U \rangle$ and $\langle T \rangle$ would not display the sharp changes that are observed.

Another way of observing motion of fluid within the interface is to produce streamlines following the vorticity surface. Velocity vectors at points interpolated onto the surface are resolved into normal and parallel components, and streamlines are drawn from the latter. The normal components would represent motion of the interface itself as it continually changes shape (but not including interface motion relative to the fluid by outwards diffusion of the vortical surface). Surface streamlines are shown in figure 16 for a small part of the unforced wake. The left-hand half of figure 15(b) is a cut through the protrusion in the middle of figure 16, but the velocity zero is placed on the upstream-facing surface in the latter case. Figure 15 gives a two-dimensional view of motion above and below the surface, while figure 16 is a ‘three-dimensional’ view of the resulting flow patterns induced along the surface. The topological pattern here is an unstable node, for which fluid at the level of the surface spreads out in all directions. The convoluted nature of the surface can also be seen in this figure.

Other areas of the surface were explored, and various topological features were found including saddles and bifurcation lines, but unstable nodes seemed to have the strongest signature. On the downstream side (not shown) of the protrusion in figure 16 there is a weakly stable node that could indicate a separation point, but the velocity of the surface normal to itself may be more significant in that area.

3.9. *Entrainment*

Boundary entrainment may be thought of as an interface moving through a fluid with a velocity E_b normal to itself. This implies that vorticity (and likewise any passive scalar) advances into irrotational fluid through molecular diffusion (Corrsin & Kistler 1955). Of course the viscous diffusive action depends on the gradients produced by the large-scale and turbulent flow fields. As with other processes of turbulence that depend locally on viscous action (e.g. drag of an obstacle or dissipation rates), the mean value of E_b , normalized on a characteristic velocity U_0 , is found to be approximately independent of the value of the Reynolds number (Townsend 1976).

Computed values of the three terms for viscous diffusion of vorticity ($\nu \nabla^2 \omega_x$, $\nu \nabla^2 \omega_y$ and $\nu \nabla^2 \omega_z$) indicate how vorticity levels are changing within fluid elements irrespective of fluid motion. Diffusion of spanwise vorticity, conditioned on vertically facing interfaces, is presented in figure 17, inverted so that the curve is positive where the magnitude of ω_z is increasing (ω_z is negative here). The interface thickness is

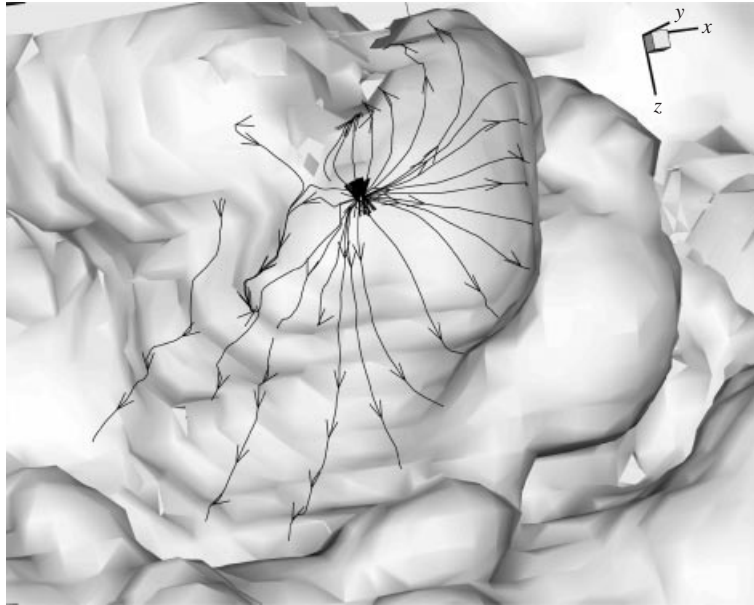


FIGURE 16. Streamlines following the vorticity surface enclosing a protrusion (see text).

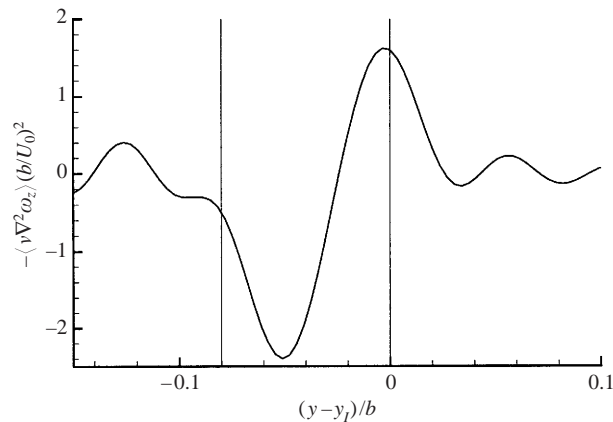


FIGURE 17. Viscous diffusion of spanwise vorticity for vertically facing interfaces, unforced wake.

delineated by vertical lines as in earlier figures. Figure 17 demonstrates that fluid right at the outer surface of the interface is undergoing the most rapid increase in the magnitude of spanwise vorticity by diffusion, and at $-0.05b$, within the interface thickness, fluid is losing spanwise vorticity (by diffusion) even more rapidly. Thus viscous action at the surface is expanding the volume of vortical fluid but also depleting the vorticity of nearby regions. Flows within the vortical regions (e.g. figure 15) replenish vorticity near the surface, and consequently the position of maximum vorticity loss by diffusion coincides very closely with the peak in $\partial\langle U\rangle/\partial y$ (figure 7a). Diffusion of streamwise vorticity is also likely to be significant at vertically facing interfaces, but cannot be assessed through the present set of detections because ω_x is equally likely to be positive or negative by symmetry.

While it would be interesting to determine whether orientation, height or angle of

the interface have an effect on entrainment rate directly from the diffusion terms, there are other cases similar to the above where symmetry precludes a meaningful result with the present sets of ω -surface detections. However, it is possible instead to get an indication from results presented earlier. At the outer surface of the interface, vorticity diffusion is directly related to the curvature of the $\langle\omega\rangle$ distribution (figures 6, 7, 11, 14). These distributions all behave in a fairly similar manner, so it is possible to say qualitatively that entrainment rate is not greatly influenced by any of the selection parameters used so far. None of the regions investigated displays, for example, an interface where fluid is entrained at a greatly reduced rate. As with all conditional averages, the properties of the individual realizations that make up the conditional results may vary considerably.

4. Implications for statistical models

As discussed in the Introduction, the turbulent kinetic energy $k = (\overline{u^2} + \overline{v^2} + \overline{w^2})/2$ and the energy dissipation rate ϵ tend to zero at the outer edge of the flow. Therefore estimates for terms used in models of Eulerian one-point statistics with k or ϵ in the denominator, such as the dissipation length scale $\ell_\epsilon = k^{3/2}/\epsilon$ or eddy viscosity $\nu_e = \ell_\epsilon k^{1/2} = k^2/\epsilon$, become ill-defined and cause numerical problems for Reynolds-averaged Navier–Stokes (RANS) computations (e.g. Cazalbou *et al.* 1994). Since such methods are steady state as far as the turbulence is concerned, the unsteady convoluted interface cannot be calculated directly, and therefore the profiles of all mean quantities are also identically the profiles at the turbulent/non-turbulent interface. One could choose to try to produce the correct mean profiles with RANS, or the correct interface, or perhaps a compromise profile, but at least one aspect of flow physics will be unrealistic. Nevertheless statistical models based on quantities such as k or ϵ are widely used for computing moments of the inhomogeneous variables in the intermittent zone. The solutions are quite uncertain because they depend sensitively on the numerical approximations involved in evaluating the variables and their derivatives. The models do not distinguish between the different dynamics on either side of the random interface or the dynamics of the interface itself. One way of examining these possible limitations is to calculate, using conditional sampling, the spatial distribution of the relevant statistical moments relative to the interface and to compare these with their conventional distribution in fixed coordinates, as shown in figure 18.

Conventional Eulerian profiles in figure 18 are plotted in terms of the fixed coordinate $y/b - \bar{h}$, chosen so that the abscissa is offset by the mean height of the turbulent/non-turbulent interface in order to facilitate comparisons with the conditional profiles. Values of \bar{k} and $\bar{\epsilon}$ are calculated directly from the DNS data, and then turbulent viscosity $\nu_t = C_\mu(\bar{k}^2/\bar{\epsilon})$ and the modelled Reynolds shear stress $(-\overline{uv})_M = \nu_t(d\bar{U}/dy)$ are obtained, where C_μ has the standard value of 0.09 (Cazalbou *et al.* 1994).

In figure 18(a) the kinetic energy of the fluctuations $\langle k \rangle$ relative to the conditional mean velocity $\langle U \rangle$ (see the discussion of $\langle u^2 \rangle$ curves in figure 8) is plotted as a function of $(y - y_I)$, i.e. relative to the interface position, and shown as a dashed line. In the non-turbulent region ($y > y_I$) these fluctuations are irrotational and do not produce any Reynolds stress (i.e. $\langle -uv \rangle \approx 0$). Even in the turbulent region ($y < y_I$) additional irrotational fluctuations are induced by the presence of the interface, to ensure that the normal velocity and pressure are continuous across the interface (Carruthers & Hunt 1986). The contribution of these fluctuations $\langle \tilde{k} \rangle$ needs to be subtracted from

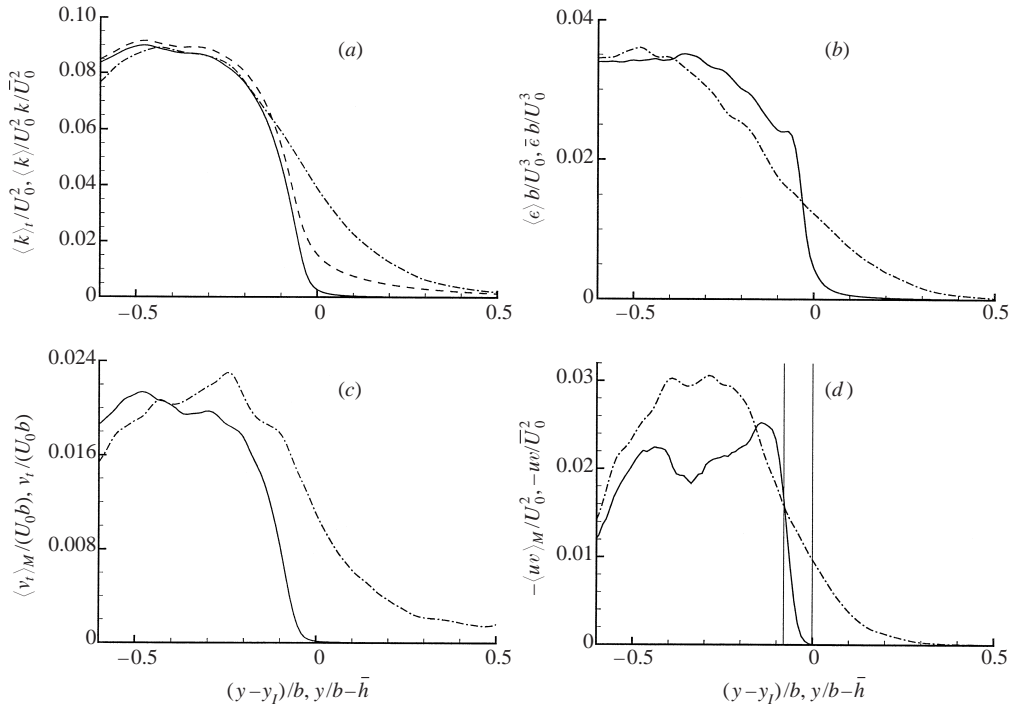


FIGURE 18. One-point statistics based on Eulerian (—) and conditional averaging, enforced wake. (a) Kinetic energy. ———, $\langle k \rangle$; ———, ‘purely turbulent’ $\langle k \rangle_t$. (b) Dissipation rate. (c) Turbulent viscosity. (d) Shear stress; interface position shown by vertical lines.

$\langle k \rangle$ in order to estimate the dynamically significant, rotationally driven component $\langle k \rangle_t$ in the turbulent region. Thus

$$\langle k \rangle_t = \langle k \rangle - \langle \tilde{k} \rangle \quad (4.1)$$

where, following Carruthers & Hunt (1986), $\langle \tilde{k} \rangle = \langle k \rangle$ for $y > y_I$, and

$$\langle \tilde{k} \rangle(y_I - y) \approx \langle \tilde{k} \rangle(y - y_I) \quad (4.2)$$

for at least the thickness of the interface below y_I . The curve of $\langle k \rangle_t$ is also plotted on figure 18(a). The conditionally sampled curve of local dissipation rate $\langle \epsilon \rangle$, plotted in figure 18(b), shows a sharp cutoff at the interface. The curve continues to rise for a little distance inside the interface, unlike that of $\langle \omega \rangle$ which immediately levels off. This is the region where $\partial \langle U \rangle / \partial y$ makes a large contribution to $\langle \omega \rangle$ (figure 7).

A model for the conditional eddy viscosity $\langle v_t \rangle$ can be estimated as in fully developed turbulent flow, i.e.

$$\langle v_t \rangle_M = C_\mu \frac{\langle k \rangle_t^2}{\langle \epsilon \rangle}. \quad (4.3)$$

The result, plotted in figure 18(c), shows that $\langle v_t \rangle_M$ is zero for $y > y_I$, because $\langle k \rangle_t$ is, by definition, zero in the non-turbulent region. In the turbulent region $\langle v_t \rangle_M$ increases fairly sharply below $y = y_I$ over a distance of about $0.2b$, similarly to $\langle k \rangle_t$ but less sharply than $\langle \epsilon \rangle$. If $\langle v_t \rangle$ is estimated in terms of an integral length scale of the normal component L_y and the normal velocity $\langle v^2 \rangle$, i.e. $\langle v_t \rangle_M = \langle v^2 \rangle^{1/2} L_y$, a similar result would be expected since both these quantities are approximately constant in the

turbulent region. The modelled Reynolds shear stress $\langle -uw \rangle_M$ for the turbulent region computed from this estimate of eddy viscosity $\langle \nu_t \rangle_M$, i.e. $\langle -uw \rangle_M = \langle \nu_t \rangle_M \partial \langle U \rangle / \partial y$, is plotted in figure 18(d), showing the expected sharp increase across the interface.

Thus the statistical models do not completely represent the dominant dynamical features for the outer edges of turbulent flows. Diffusive modelling describes the turbulent transfer of momentum or scalars towards the interface, but the processes at the interface, where an intense convoluted and randomly moving vortex sheet causes the interface to move into the quiescent fluid outside it, are not described well by such models. Computationally they are unsatisfactory because the results for E_b depend on the numerical scheme and the grid size (Large *et al.* 1994; Hunt *et al.* 2001). With regard to the interface itself, Cazalbou *et al.* (1994) investigated certain statistical methods at free-shear edges with various combinations of values for the coefficients taken from the literature. They found results that (qualitatively) span the full range given by figure 18, from a sharp cutoff or discontinuity to a smooth decay. Thus with appropriately chosen coefficients such statistical models might indeed reproduce the sharp interface properties described here. However the models cannot represent satisfactorily the statistics of the fluctuations, or the mean field where there are gradients of scalars in the external quiescent fluid (e.g. Durbin, Hunt & Firth 1982).

In large-eddy simulations (LES) the large-scale fluctuations of the interface are computed together with an approximation of the small-scale turbulence, so the broad features of the interface are represented as well as the mean statistics. However the local dynamics at the interface at scales smaller than the grid size (or filter size) are not represented in LES, which may be a source of error in the calculations of entrainment, mixing and reaction rates at these interfaces. Better resolution may be required at interfaces than is sometimes assumed in LES applications.

5. Concluding remarks

The detailed study using DNS of the ensemble statistics of the mean and fluctuating flow variables near the interface of the outer edge of turbulent wakes has provided new evidence for the characteristic features of the flow that have been inferred from previous experimental research. It is clear that the interface is thin and generally continuous, and separates rotational motions that are rather homogeneous from irrotational motions that are very inhomogeneous; there is a significant jump in mean velocity ΔU and temperature ΔT across the thickness of the interface ℓ_I ($< 0.1b$); the vorticity jump across the interface is of the same order as the modulus of vorticity in the bulk of the turbulent region. Inspection of the conditional flow structure around the interface suggests that the large-scale engulfing motions mainly determine the mean entrainment rate, even though small-scale mixing of vorticity plays an essential part in the whole process. Since the large-scale motions are not locally determined, this explains why entrainment rates are sensitive to external forcing and to the structure of large-scale eddy motion. Conversely it means that local statistical models, e.g. those based on the diffusion approximation, do not represent the physical processes.

The first aspect of the interface that emerged from this study is that the interface remains thin both as a result of the kinematic vorticity advection around the nodal stagnation points and the enfolding saddle points where any vorticity that diffuses from the interface is re-entrained, and as a result of bulging and stretching of the interface. Secondly, vorticity components are *amplified* at the interface as the turbulent eddies move outwards into the non-turbulent flow. This amplification is greater where the mean vorticity is non-zero as in these wakes, and where there is a net outward

movement of the interface (i.e. $E_b > 0$). The third point is that the properties of the interface (including the direct effects of mean shear) are largely independent of the direction in which the interface is facing and its distance from the centreplane.

In all flows the irrotational velocity fluctuations in the external non-turbulent region are described by the theory of Phillips (1955). But the turbulence structure within the turbulent region near the interface is affected by the mean vorticity in the flow and by the mean movement of the interface. This is why the idealized theory of Carruthers & Hunt (1986) for homogeneous unshered turbulence near a non-entraining interface does not provide a quantitative description of the turbulence in this flow. But it does show qualitatively how the velocity fluctuations within the turbulent region are affected by the fluctuating vortex sheet on the interface and the irrotational fluctuations outside it.

A more specific theory is needed to account for the inhomogeneous production of turbulent energy in the turbulent region near the interface. Also the highly indented form of the interface leads to straining motions that anisotropically distort the small-scale turbulence. Both these effects could perhaps be modelled using rapid distortion theory applied to the conditional flow field in the turbulent region. Also there are similarities in these mechanisms with the energy production 'balances' derived from conditional sampling measurements in the large eddies of mixing layers, wakes etc. (Hussain 1986; Antonia *et al.* 1987a).

An interesting conclusion to be drawn from the present results is that the intermittent zone between turbulent and non-turbulent motion is likely to be less energetic and more diffuse for flows with lower mean shear across the interface. Such a case occurs in the diffusion of turbulent puffs or plumes with no internal mean motion (e.g. Townsend 1976). However, large-scale turbulent motions are likely to produce *locally* sheared regions in which a typical interface exists for a finite time; this may provide the basis for analysis of turbulent entrainment in the absence of mean shear.

Further analyses of flow dynamics around the interface will be presented in a future paper. They include an assessment of Prandtl mixing length theory in relation to the interface, results for turbulent Prandtl number, and a relation between Reynolds shear stress $\langle -uw \rangle$ and the product of $\Delta \langle U \rangle$ and E_b .

Note added in proof: Results from experiments by Westerwed *et al.* (2001) are in good agreement with the present work.

REFERENCES

- ALEXOPOULOS, C. C. & KEFFER, J. F. 1971 Turbulent wake in a passively stratified fluid. *Phys. Fluids* **14**, 216–224.
- ANTONIA, R. A., BROWNE, L. W. B., BISSET, D. K. & FULACHIER, L. 1987a A description of the organized motion in the turbulent far-wake of a cylinder at low Reynolds number. *J. Fluid Mech.* **184**, 423–444.
- ANTONIA, R. A., SHAH, D. A. & BROWNE, L. W. B. 1987b The organized motion outside a turbulent wake. *Phys. Fluids* **30**, 2040–2045.
- BISSET, D. K., ANTONIA, R. A. & BROWNE, L. W. B. 1990 Spatial organization of large structures in the turbulent far-wake of a cylinder. *J. Fluid Mech.* **218**, 439–461.
- BISSET, D. K., HUNT, J. C. R., CAI, X. & ROGERS, M. M. 1998 Interfaces at the outer boundaries of turbulent motions. *Annual Research Briefs 1998*, pp. 125–135. Center for Turbulence Research, Stanford University.
- CARRUTHERS, D. J. & HUNT, J. C. R. 1986 Velocity fluctuations near an interface between a turbulent region and a stably stratified layer. *J. Fluid Mech.* **165**, 475–501.

- CAZALBOU, J. B., SPALART, P. R. & BRADSHAW, P. 1994 On the behaviour of two-equation models at the edge of a turbulent region. *Phys. Fluids* **6**, 1797–1804.
- CHEN, C.-H. P. & BLACKWELDER, R. F. 1978 Large-scale motion in a turbulent boundary layer: a study using temperature contamination. *J. Fluid Mech.* **89**, 1–31.
- CORRSIN, S. 1943 Investigation of flow in an axially symmetrical heated jet of air. *NACA WR W-94*. NACA, Washington DC.
- CORRSIN, S. & KISTLER, A. L. 1955 Free-stream boundaries of turbulent flows. *NACA TR 1244*. NACA, Washington DC.
- DURBIN, P. A., HUNT, J. C. R. & FIRTH, D. 1982 Mixing by a turbulent wake of a uniform temperature gradient in the approach flow. *Phys. Fluids* **25**, 588–591.
- FABRIS, G. 1979 Conditional sampling study of the turbulent wake of a cylinder. Part 1. *J. Fluid Mech.* **94**, 673–709.
- FERRE, J. A., MUMFORD, J. C., SAVILL, A. M. & GIRALT, F. 1990 Three-dimensional large-eddy motions and fine-scale activity in a plane turbulent wake. *J. Fluid Mech.* **210**, 371–414.
- GARTSHORE, I. S., DURBIN, P. A. & HUNT, J. C. R. 1983 The production of turbulent stress in a shear flow by irrotational fluctuations. *J. Fluid Mech.* **137**, 307–329.
- HUNT, J. C. R., ABELL, C. J., PETERKA, J. A. & WOO, H. 1978 Kinematical studies of the flow around free or surface-mounted obstacles; applying topology to flow visualization. *J. Fluid Mech.* **86**, 179–200.
- HUNT, J. C. R., VASSILICOS, J. C., SANDHAM, N., LAUNDER, B. E., MONKEWITZ, P. A. & HEWITT, G. 2001 Developments in turbulence research: a review based on the 1999 programme of the Isaac Newton Institute, Cambridge. *J. Fluid Mech.* **436**, 353–391.
- HUSSAIN, A. K. M. F. 1986 Coherent structures and turbulence. *J. Fluid Mech.* **173**, 303–356.
- HUSSAIN, A. K. M. F. & CLARK. 1981 On the coherent structure of the axisymmetric mixing layer – a flow-visualization study. *J. Fluid Mech.* **104**, 263–294.
- KOVASZNAY, L. S. G., KIBENS, V. & BLACKWELDER, R. F. 1970 Large-scale motion in the intermittent region of a turbulent boundary layer. *J. Fluid Mech.* **41**, 283–325.
- LARGE, W. G., MCWILLIAMS, J. C. & DONEY, S. 1994 Oceanic vertical mixing: a review and a model with non-local boundary layer parameterisation. *Rev. Geophys.* **23**, 363–403.
- LARUE, J. C. & LIBBY, P. A. 1974 Temperature fluctuations in the plane turbulent wake. *Phys. Fluids* **17**, 1956–1967.
- MONIN, M. & YAGLOM, A. 1971 *Statistical Fluid Mechanics*. MIT Press.
- MOSER, R. D., ROGERS, M. M. & EWING, D. W. 1998 Self-similarity of time-evolving plane wakes. *J. Fluid Mech.* **367**, 255–289.
- PERRY, A. E. & CHONG, M. S. 1987 A description of eddy motions and flow patterns using critical-point concepts. *Annu. Rev. Fluid Mech.* **19**, 125–155.
- PHILLIPS, O. M. 1955 The irrotational motion outside a free boundary layer. *Proc. Camb. Phil. Soc.* **51**, 220.
- SREENIVASAN, K. R. & MENEVEAU, C. 1986 The fractal facets of turbulence. *J. Fluid Mech.* **173**, 357–386.
- STEINER, T. R. & PERRY, A. E. 1987 Large-scale vortex structures in turbulent wakes behind bluff bodies. Part 2. Far-wake structures. *J. Fluid Mech.* **174**, 271–298.
- STRANG, E. J. 1997 Entrainment and mixing in stratified shear flows. PhD thesis, Arizona State University.
- TOWNSEND, A. A. 1948 Local isotropy in the turbulent wake of a cylinder. *Austral. J. Sci. Res. A* **1**, 161–174.
- TOWNSEND, A. A. 1949 The fully developed turbulent wake of a circular cylinder. *Austral. J. Sci. Res. A* **2**, 451–468.
- TOWNSEND, A. A. 1976 *The Structure of Turbulent Shear Flow*, 2nd edn. Cambridge University Press.
- TURNER, J. S. 1973 *Buoyancy Effects in Fluids*. Cambridge University Press.
- TURNER, J. S. 1986 Turbulent entrainment: the development of the entrainment assumption, and its application to geophysical flows. *J. Fluid Mech.* **173**, 431–471.
- WESTERWEEL, J., HOFMANN, T., FUKASHIMA, C. & HUNT, J. C. R. 2001 Experimental investigation of the turbulent/non-turbulent interface at the outer boundary of a self-similar turbulent jet. *Proc. 4th Intl Symp. on Particle Image Velocimetry, Goettingen 17–19 Sept 2001*.
- WYGNANSKI, I. & FIEDLER, H. E. 1970 The two-dimensional mixing region. *J. Fluid Mech.* **41**, 327–361.